Published in IET Microwaves, Antennas & Propagation
Received on 20th December 2007
Revised on 23rd July 2008
doi: 10.1049/iet-map:20070352

In Special Issue on Asia Pacific Microwave Conference 2007

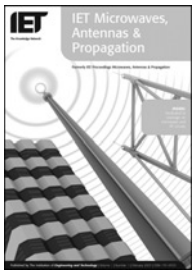

ISSN 1751-8725

Quasi-elliptic dual-band filter design using stepped-impedance resonators and coupling topologies for narrow-to-wide-band applications

Marjan Mokhtaari[1] *Jens Bornemann*[1] *Smain Amari*[2]

[1]*Department of Electrical and Computer Engineering, University of Victoria, PO Box 3055, Victoria, BC, Canada V8W 3P6*
[2]*Department of Electrical and Computer Engineering, Royal Military College of Canada, 17000 Station Forces, Kingston, ON, Canada K7K 7B4*
E-mail: marjan@uvic.ca

Abstract: Design guidelines are presented for new planar quasi-elliptic dual-band filters in applications requiring high performance, compact size, ease of fabrication and integration with remaining circuitry. Novel coupling topologies between folded stepped-impedance resonators (SIRs) are utilised to generate two narrow or two wide passbands at desired centre frequencies with multiple attenuation poles between passbands. Source–load coupling is employed to place additional attenuation poles within the lower and upper stopband regions. The main feature of these dual-band filters is their approximately symmetrical response, including high selectivity of each passband and controllable fractional bandwidths for either narrowband or wideband coupling schemes, respectively. In addition, the simplicity of the design approach and the use of folded SIR structures result in compact size. Several microstrip dual-band filters in various cascaded SIR configurations with narrow or wide passbands are designed and measured. The measured results are in very good agreement with those obtained from different electromagnetic simulation packages such as Ansoft Designer and IE3D.

1 Introduction

Dual-band filters find many applications in wireless communication systems, and general filter synthesis approaches address the design of dual-band coupled resonator topologies [1, 2]. Planar dual-band filter designs rely on the harmonic tuning properties of stepped-impedance resonators (SIRs) [3]. Especially the second resonance of such resonators can be efficiently used to create dual-band filters [4–11]. Alternatively, including the third resonance, SIRs are employed in triple-band filters [12, 13] or ultra-wideband (UWB) filters [14–17].

In order to create dual-band filters of varying bandwidths, multiple SIRs are connected and their coupling is appropriately adjusted. Therefore the design of coupling coefficients for cascaded SIRs is of fundamental importance [5, 15, 18]. However, the type of coupling between SIRs mainly determines the individual bandwidths and therefore influences the realisation of coupling coefficients [19, 20]. In certain coupling schemes, the coupling in the second passband cannot be controlled efficiently, or harmonic passbands cannot be suppressed effectively. Moreover, coupling schemes realised by different coupled-line segments can contribute to additional attenuation poles between the passbands or outside of the passbands [10, 20] or, alternatively, can create additional resonances within the filter bands to increase bandwidth [14, 16, 19].

This paper utilises coupling coefficients to determine the filter performances in the principle passbands of SIR dual-band filters. The number and location of attenuation poles as well as the two bandwidths of such quasi-elliptic dual-band filters are designed according to coupling schemes,

which vary in topology for narrowband to wideband applications. Moreover, the use of source–load coupling generates additional attenuation poles, especially those located in the lower and upper stopbands, that is, to the left of the lower passband and to the right of the upper passband.

Section 2 presents the design theory and introduces the coupling topologies. In Section 3, six design examples in microstrip technology are presented and verified by prototyping and measurements.

2 Theory

Fig. 1*a* shows the basic configurations of a microstrip SIR. Fig. 1*b* depicts its folded version that has both high- and low-impedance segments converted into two parallel sections, whose impedances are twice of those in Fig. 1*a*. The open-ended high-impedance lines in Fig. 1*b* can provide tighter coupling between coupled-line sections of adjacent SIRs in order to approach filter characteristics with extended bandwidth. Moreover, they contribute to a size reduction of the final filter structure.

As is well known, the resonance frequencies of a single SIR element can be calculated from

$$R_z - \tan\theta_1 \tan\theta_2 = 0, \quad \text{odd mode} \tag{1a}$$

$$R_z \tan\theta_1 + \tan\theta_2 = 0, \quad \text{even mode} \tag{1b}$$

where $R_Z = Z_2/Z_1$ is the impedance ratio and θ_1 and θ_2 are the electrical lengths of the low- and high-impedance segments, respectively. The fundamental and harmonic frequencies occur alternatively in the odd and even modes. The ratio of the higher-order resonance frequencies to that of the fundamental mode can be determined through (1) in terms of R_Z and U, which is expressed as the electrical length ratio:

$$U = \frac{\theta_2}{\theta_1 + \theta_2} \tag{2}$$

Note that the actual lengths $[L_2/(L_1 + L_2) \simeq \theta_2/(\theta_1 + \theta_2)]$ depend on the effective permittivities, discontinuity and open-end effects.

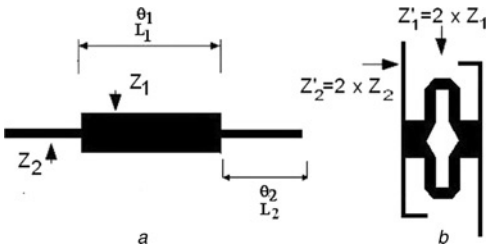

Figure 1 *Two configurations of an SIR structure*

a Basic

b Advanced with folded low-impedance segments and parallel open-ended high-impedance segments

Fig. 2 shows the ratio of the harmonic frequencies to the fundamental mode (f_n/f_1) of a basic SIR as a function of the electric length ratio (U) for different, arbitrarily selected impedance ratios (R_Z). In the synthesis of a single dual-band SIR in Fig. 1, the centre frequencies of the first and second passbands are recognised as the fundamental and first higher-order resonances, respectively. The viable solutions for the length ratios of the SIR are typically determined through Fig. 2 in terms of a given R_Z. Clearly, for a specific resonance ratio (e.g. $f_2/f_1 = 1.7$ as shown in Fig. 2), two different solutions can be selected for the length ratio in terms of each impedance ratio. They are referred to in Fig. 2 as B and C for $R_Z = 1.55$ and A and D for $R_Z = 3.5$. The optimum solution for the length ratio is usually specified by the fact that the next higher harmonic should appear at a frequency, which is as far away as possible from the second passband. However, in view of fabrication and size reduction, realisable impedance characteristics of the low- and high-impedance segments in the SIR topology must be considered.

The response of an SIR bandpass filter with bandwidth Δf and centred at frequency f_0 is determined by a coupling matrix, whose elements represent the normalised coupling coefficients between individual SIRs as well as those to the input/output ports. The actual coupling coefficients k_{ij} are obtained from

$$k_{01} = k_{N,N+1} = M_{01}\sqrt{\frac{\Delta f}{f_0}}$$

$$k_{ij} = k_{ji} = M_{ij}\frac{\Delta f}{f_0}, \quad i, j = 1, \ldots, N; \quad i \neq j \tag{3}$$

where N is the number of resonators in the filter topology and $i = 0$ and $j = N+1$ refer to the input and output ports, respectively. The coupling values between coupled-line sections are determined via even/odd-mode impedance

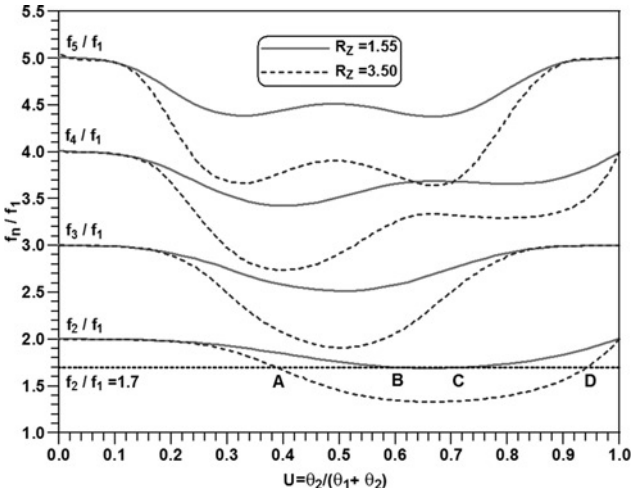

Figure 2 *Harmonic to fundamental mode ratio of a basic SIR as functions of length and impedance ratios*

doi: 10.1049/iet-map:20070352

characteristics

$$k_{ij} = \frac{Z_{0e} - Z_{0o}}{Z_{oe} + Z_{0o}} \quad (4)$$

and are designed to match those from (3).

Fig. 3 shows various open-ended coupled-line segments between resonators and input/output ports and their equivalent impedance inverter circuit in a dual-band filter scheme (Fig. 3*d*). Fig. 3*a* represents the coupling section to produce passbands with narrow bandwidth. The coupling segments in Figs. 3*b* and 3*c* are implemented to create passbands with wider bandwidths in each band. They are similar to the coupling segments employed in UWB filters [14, 16] and are capable of producing an additional reflection zero (pole) within the band. Note that the UWB designs in [14, 16] use two coupling sections, one each to the input and output and therefore, create two reflection zeros. The coupling configurations in Figs. 3*b* and 3*c* show one coupling section linking two SIRs. Hence, they generate one reflection zero, and the open-ended stubs in Fig. 3*c* produce one transmission zero each between passbands.

Assuming that several SIRs (e.g. Fig. 1*a*) are used in a parallel-coupled-line arrangement at the fundamental resonance frequency, then such resonators have strong electric coupling at both ends and magnetic coupling at the centre of the transmission lines. At the first harmonic resonance frequency, due to the decrease in wavelength, the magnetic coupling at the centre converts to electrical coupling, thus changing completely the coupling coefficient for the second pass-band and making independent tuning impossible. Therefore an appropriate coupling choice for dual-band filters is to utilise the inter-coupled open-ends of SIRs (c.f. Figs. 3*a*–3*c*) so that the coupling in both passbands is electric.

In the design of a narrowband dual-band filter, the coupling matrix is generally synthesised using the centre frequency of the first passband (f_1) and the desired bandwidth (Δf). Due to the electric coupling topology between open-ended high-impedance coupling segment in Fig. 3*a* and the theoretically frequency-independent characteristics of the coupling matrix elements for narrow bandwidths, it is assumed that the coupling coefficients remain approximately constant for the second passband as well; therefore the same coupling matrix is utilised to represent both passbands.

Unfortunately, the situation is different for the coupling sections shown in Figs. 3*b* and 3*c*. Their coupling is still electric but, used over a broad frequency range, it is no longer frequency-independent. Therefore, the coupling matrix concept cannot be demonstrated for wide dual-band filter designs. Besides, the coupling segment in Fig. 3*c* represents not only a coupling element but also an additional resonator within the passband. Hence, the number of coupled-line segments shown in Fig. 3*c* increases the order of the filter, which provides extra bandwidth.

In order to isolate both bands, at least one attenuation pole must be produced and located between passbands. The coupled-line section in Fig. 3*a* and the folded open-ended high-impedance transmission line in Fig. 3*c* can generate attenuation poles between passbands if the electrical length θ_2 is selected as a quarter-wavelength at the overall centre frequency, which is an arithmetic mean of the centre frequencies of both passbands. The length of the low-impedance segment θ_1 in a basic SIR and the appropriate impedance ratio R_Z can then be extracted from the graph in Fig. 2.

Fig. 4 shows three dual-band filter structures using three cascaded SIRs for narrow bandwidth applications. Fig. 4*a* depicts the standard centre section of an SIR (c.f. Fig. 1*a*) whereas in Figs. 4*b* and 4*c*, the folded resonator in Fig. 1*b* is utilised which reduces the sizes of those filters to about

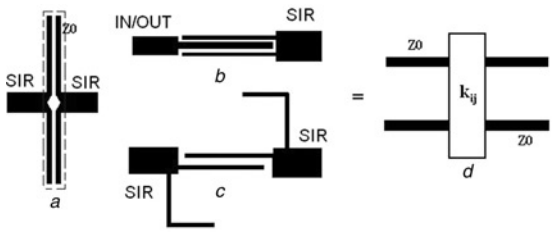

Figure 3 *Various open-ended coupled-line sections*
a Narrow bandwidth
b Wide bandwidth
c In each passband of a dual-band filter
d Equivalent impedance inverter circuit

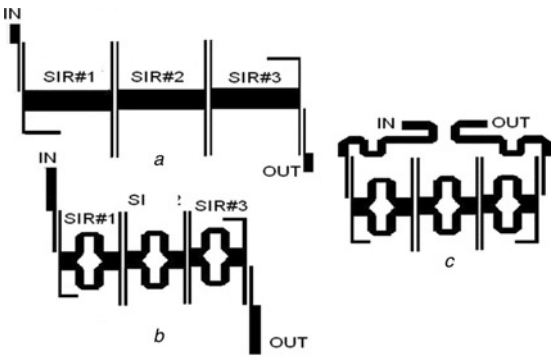

Figure 4 *Dual-band filter structures with three cascaded SIRs for narrow bandwidth applications*
Coupling according to Fig. 3*a*
a Parallel open-ended high-impedance sections only
b Additional parallel low-impedance sections
c Including source–load coupling

60% of that in Fig. 4*a*. Fig. 4*c* also shows source–load (input–output) coupling to introduce attenuation poles in the leftmost and rightmost stopbands of the dual-band filter.

As arbitrary examples, consider the SIRs shown in Figs. 4*a* and 4*b*. In order to be able to work with that in Fig. 2, let us assume that $f_2/f_1 = 1.7$ and that $f_1 = 2.3$ GHz, thus $f_2 = 3.9$ GHz. For this dual-band filter, the graph in Fig. 2 demonstrates that several length ratios, indicated as A–D, can be extracted in terms of two different impedance ratios ($R_z = 1.55$ and $R_z = 3.5$). The higher impedance ratio requires either thicker low-impedance or thinner high-impedance segments, which means a larger structure of an SIR as well as rough and intricate fabrication. Therefore the length ratios indicated as A and D in Fig. 2 are eliminated. The frequency ratios of the second and third higher resonance frequencies to the fundamental mode (f_3/f_1 and f_4/f_1) are the key components to select an appropriate solution for the length ratio (U), since they ultimately lead to a filter response with extended upper rejection band.

As indicated in Fig. 2, the ratio of the second harmonic frequency to the fundamental mode (f_3/f_1) is 2.1 and 2.6, and the ratio of the third harmonic frequency (f_4/f_1) equals 3.25 and 3.5 for points B and C, respectively. Consequently, point C ($U = 0.67$, $R_Z = 1.55$) in Fig. 2 is the best solution. The substrate is RT6010 with relative permittivity $\varepsilon_r = 10.2$ and substrate thickness $h = 25$ mils. The length of the high-impedance coupling segment is a quarter-wavelength ($\simeq$9.2 mm) at $f_0 = \sqrt{f_1 f_2} = 3.0$ GHz. Therefore the length of the low-impedance segment of the SIR can be calculated through the specified length ratio ($U = 0.67$) in Fig. 2. The impedance characteristic of the high-impedance segment (Z_2) of the basic SIR is selected as 40 Ω for all filter structures so that parallel high-impedance segments in Fig. 1*b* and 1*c* are at 80 Ω. The respective value of the low-impedance segment (Z_1) of the SIR is calculated by the specified impedance ratio ($R_Z = 1.55$) such that $Z_1 = 26$ Ω.

Let us further assume that the 10 dB bandwidths of the dual-band filter be 300 MHz in each passband. Three cascaded single-element SIRs depicted in Figs. 4*a* and 4*b* are used to cover the dual-band filter specifications, including the desired bandwidth in each passband and a high isolation between bands. The normalised coupling matrix of the three-pole filter is

$$M = \begin{bmatrix} 0 & 1.035 & 0 & 0 & 0 \\ 1.035 & 0 & 0.947 & 0 & 0 \\ 0 & 0.947 & 0 & 0.947 & 0 \\ 0 & 0 & 0.947 & 0 & 1.035 \\ 0 & 0 & 0 & 1.035 & 0 \end{bmatrix} \quad (5)$$

Finally, the gaps between the open-ended coupled-line sections and the input/output paths are determined by matching the actual coupling elements with those of the coupling matrix for the desired bandwidth and centre frequency according to (3) and (4). The gap between individual coupled-line sections is varied using the closed-form expressions in [21] until a coupling value is obtained which equals the respective entry in the coupling matrix. In our experience, fine-tuning of about 5–10% of the synthesised dimensions might have to be applied to adjust all interactions between the elements involved. Thus, the initial design is sufficient to employ standard optimisation techniques or trial-and-error procedures on the coupled-line sections. Note that as long as the individual passbands are narrow, this design approach (in terms of coupling matrix and appropriate selection of impedance ratios) can be employed for any dual-band filter and is not limited to applications where the two passbands are close to each other. For wide-bandwidth applications, however, the design is restricted to dual-band filters with nearby passbands. This is due to the coupling segments and the equal-length open stubs which sufficiently represent reflection and transmission zeros only near the centre frequency.

Fig. 5 shows the comparison of the performances of the actual dual-band filters in Figs. 4*a* and 4*b* with the performance of the coupling matrix of (5) in each passband. The simulation results are in line with the theoretical response of the coupling matrix within each passband. The computed insertion loss is <2 dB, and the return loss is better than 10 dB in each passband. The simulated 10 dB bandwidths are 300 and 350 MHz for the first and second passbands, respectively. The additional bandwidth on the second passband is due to the frequency-dependence of the coupled-line sections in the filter structure, which is ignored in the dual-band filter synthesis. Three transmission zeros at 2.75, 3 and 3.25 GHz are generated between the passbands due to the coupled quarter-wavelength open-ended high-impedance segments. The resonance peaks at 6 and 8.3 GHz are due to the second and third harmonics of the folded SIR (f_3 and f_4)

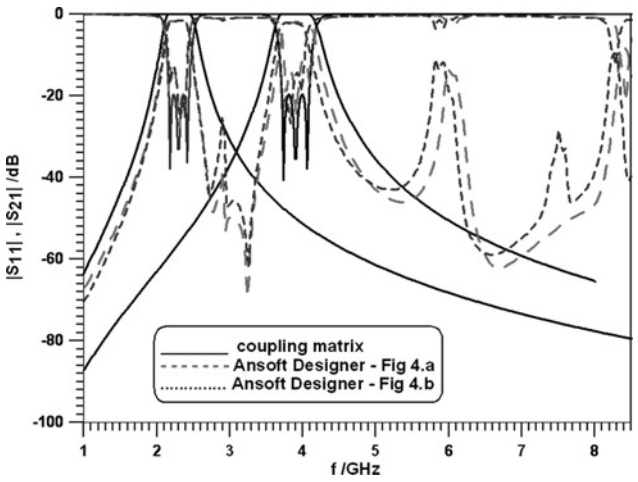

Figure 5 *Performances of the dual-band filter structures of Fig. 4a (dashed lines) and Fig. 4b (dotted lines) with those obtained from the individual coupling matrices (solid lines)*

doi: 10.1049/iet-map:20070352

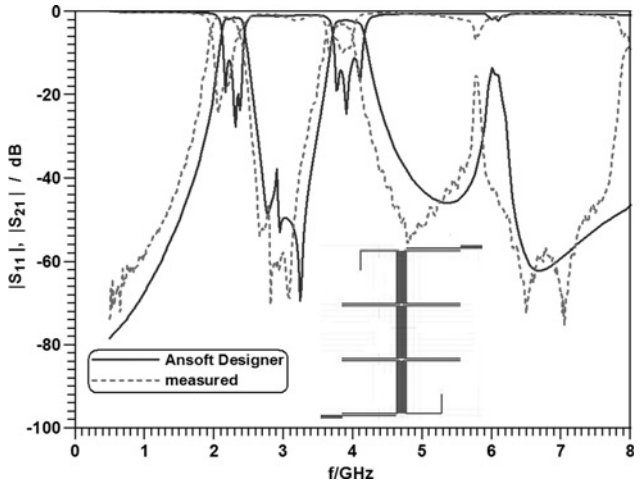

Figure 6 *Simulated and measured performances of a dual-band filter using a three-cascaded SIR configuration according to Fig. 4a*

as indicated in Fig. 2. The spurious passband at 7.5 GHz for the performance of the filter structure in Fig. 4*b*, which is below −27 dB, exists for all filter structures using the new folded low-impedance SIR configuration (see also the next section) and is attributed to coupling between the high-impedance and the folded low-impedance segments in the structure shown in Fig. 1*b*. This is evidenced, for example, by comparing Fig. 6 with Fig. 7. The filter in Fig. 6 uses straight, instead of folded low-impedance sections and therefore the peak at 7.6 GHz disappears. Hence, this peak appears to be a direct consequence of miniaturisation.

3 Results

This section presents some examples of dual-band filters, which have been synthesised, fabricated and measured. The results of both narrowband and wideband prototypes verify the design process described above. Note that the publication of all dimensions of the filters presented in this paper is prohibitive due to lack of space. Please contact the first author for actual dimensions of individual filters.

3.1 Dual-band filters for narrowband applications

Figs. 6 and 7 confirm the operations of the dual-band filter configurations in Figs. 4*a* and 4*b*, respectively. A good general agreement is observed between simulations and measurements. However, in both figures (as well as all following ones), a shift of the measured performances towards lower frequencies occurs. A tolerance analysis (not shown here) shows that this shift is mainly attributed to the fabrication of the coupling slots. With slot widths in the order of 100 μm and fabrication tolerances of up to 25 μm, under-etching significantly moves the measured filter response towards lower frequencies. This is a disadvantage of the proposed coupling schemes but is common to most planar filter structures requiring tight coupling for UWB or multi-band operation. Moreover, in cascaded arrangements, where the high-impedance lines branch off as shown in Fig. 3*a*, two wider-line sections are fairly close to each other and produce small but unwanted coupling. This is the main cause for the spurious response between the two passbands in Figs. 6 and 7. To a lesser degree, this coupling is also present in Fig. 8, but it vanishes for the structures in Figs. 9–11, which employ different coupling schemes between the SIRs. A size comparison between the two filters in Figs. 6 and 7 shows that the structure in Fig. 7 occupies only 60% of the substrate area size compared with that in Fig. 6.

The dual-band filters in these examples exhibit multiple attenuation poles between the two passbands. With respect

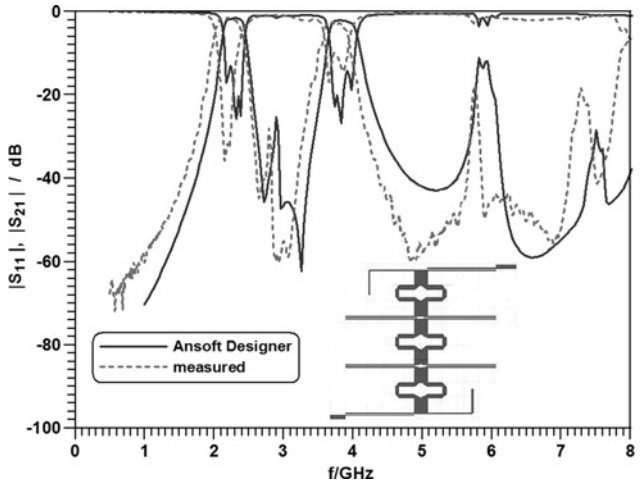

Figure 7 *Simulated and measured performances of a dual-band filter using a three-cascaded SIR configuration according to Fig. 4b*

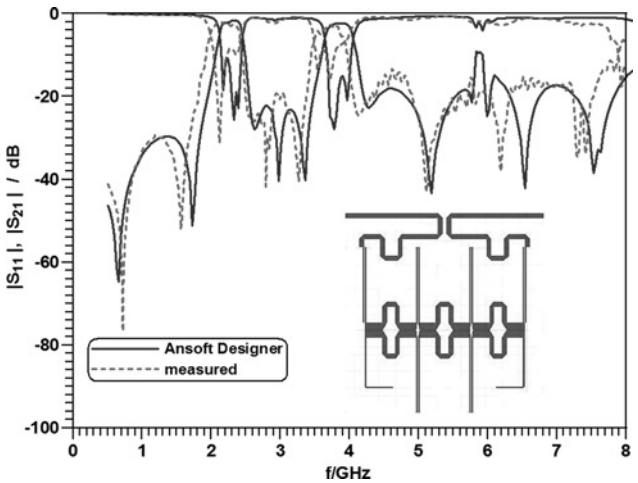

Figure 8 *Simulated and measured performances of the source–load coupled version of the dual-band filter in Fig. 7.*

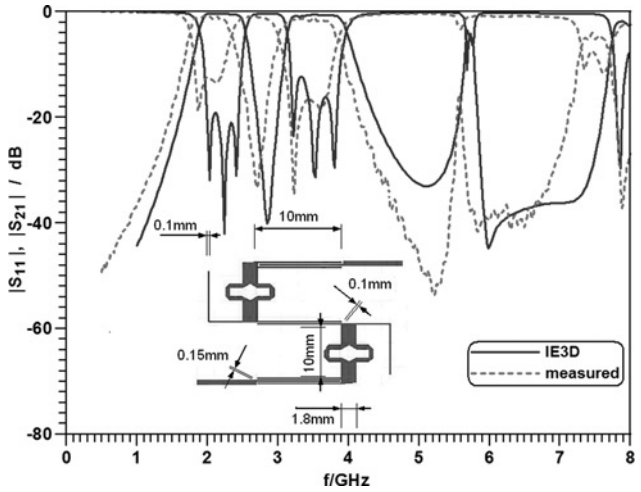

Figure 9 *Simulated and measured performances of a three-pole dual-band filter using the two cascaded SIRs from Fig. 1b and a coupled-line segment from Fig. 3b*

Structural layout and important dimensions are depicted in the inset

to the design theory, however, attenuation poles in the lower and/or upper rejection bands are not considered (although a number of attenuation poles appear in the upper bands of the measurements and are attributed to the measurement setup).

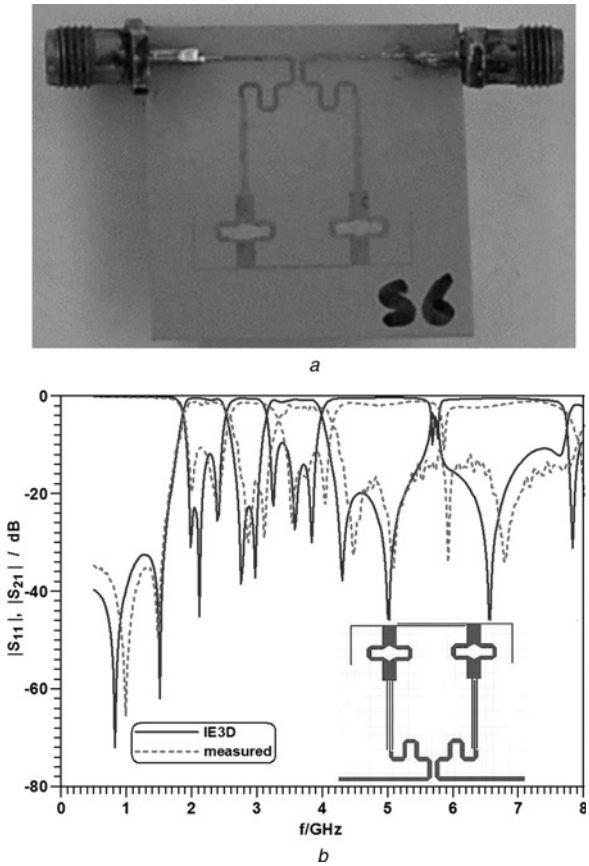

Figure 10 *Fabricated prototype (a) and simulated and measured performances (b) of the source–load-coupled version of the dual-band filter in Fig. 9*

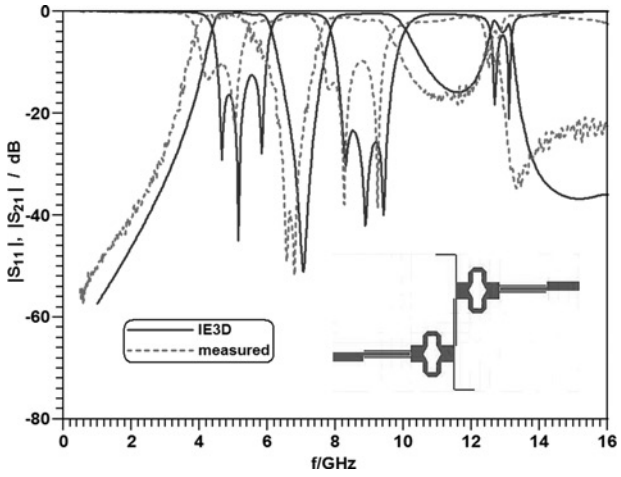

Figure 11 *Simulated and measured performances of a three-pole dual-band filter using two cascaded SIRs of Fig. 1b and coupled-line sections of Fig. 3c for $f_0 = 7$ GHz*

Source–load coupling is capable of generating additional attenuation poles in the upper and lower stopband regions. The location of such poles is primarily dependent on the value and type (electric or magnetic) of the source–load coupling. Due to unavailable coupling topologies for a multi-harmonics single-element SIR, the number of poles generated by source–load coupling is as yet unpredictable.

Fig. 8 shows the performance of the dual-band filter in Fig. 7 when source–load coupling is employed (c.f. Fig. 4*c*). Two transmission zeros on the left side of the first passband – at 0.7 and 1.65 GHz – and seven transmission zeros on the right side of the second passband – at 4.25, 5.2, 5.8, 6.1, 6.5 and 7.6 GHz – are apparently generated by the source–load coupling. The number of attenuation poles appearing in the lower rejection band does not necessarily change with additional resonators; however, source–load coupling eventually increases the number of attenuation poles in the upper stopband and thus significantly improves the rejection in this frequency range. Although the dimensions of the dual-band filter in Fig. 7 remain unchanged in Fig. 8, except for the additional source–load coupling, the latter has also a minor impact on the locations of the multiple poles between the passbands.

A comparison between Figs. 7 and 8 confirms the sharp selectivity of each passband by allocating attenuation poles in the lower/upper stopbands through source–load coupling. It also adjusts the poles between the bands and moves them slight outwards, which increases the selectivity of each passband. Due to the additional path between source and load, the general (across the frequency range) attenuation level in Fig. 8 is lower than that in Fig. 7.

3.2 Dual-band filters for wideband applications

The dual-band filter design for wideband applications is mainly based on the design of UWB filters [14, 16]. The

doi: 10.1049/iet-map:20070352

coupling configuration in Fig. 3*c* can generate two attenuation poles within an ultra-wide bandwidth due to the folded high-impedance segments, whose lengths are a quarter-wavelength at centre frequency f_0. The design procedure is the same as that demonstrated in the last section for narrow dual-band filter, but it considers the additional reflection zero in each band due to the fact that the quarter-wavelength coupled-line section acts as an extra resonator [14]. Thus, the filter shown in the inset in Fig. 9 creates one reflection zero in each passband, which are due to the centre coupled line section (one reflection zero) and those at the input and output (one double reflection zero). Since these sections must be similar in length in order to operate in both frequency bands, the two passbands for such designs must be close together, as already mentioned in Section 2. The proposed input/output-coupling segment in Fig. 3*b* also eliminates the required tight coupling in traditional UWB filters and reduces high-precision fabrication requirements due to wider coupling slots.

Fig. 9 shows the simulated and measured performances of a three-pole dual-band filter using two SIRs and quarter-wavelength coupled-line sections as resonators. The circuit depicted in the inset in Fig. 9 is fabricated on RT6010 substrate material of height $h = 25$ mils. The main line and slot widths and lengths are also shown in order to provide design engineers with some typical dimensions for the dual-band filters presented in this paper. Please note that coupling slots and line widths are at least 0.1 mm wide which is suitable for standard fabrication techniques. The centre frequencies of the first and second passbands in Fig. 9 are theoretically assumed to be $f_1 = 2.2$ GHz, $f_2 = 3.5$ GHz ($f_2/f_1 = 1.6$) with a 10 dB bandwidth of 600 MHz. However, as mentioned earlier, the bandwidth in the upper band is increased to 700 MHz due to the frequency dependence of the coupling coefficients. The centre frequency of the entire filter is located at $f_0 = 2.85$ GHz, which specifies the physical lengths of the high-impedance coupling segment to be a quarter-wavelength. The length and impedance ratios of the resonators employed in the filter structure are determined based on the graphs in Fig. 2.

A good agreement is observed between simulations and measurement. The insertion loss is <2 dB and the return loss is better than 10 dB in both bands. The slight frequency shift in the measured results is due to fabrication tolerances as explained earlier in this section. The spurious bands at 5.8 and 7.8 GHz represent the second and third harmonic modes of the employed SIRs, respectively, which – for this design – is the maximum possible distance from the second band due to the length and impedance ratios in Fig. 2.

Fig. 10 shows a photograph and the performance of the dual-band filter in Fig. 9 with added source–load coupling, which is predominantly inductive due to the interaction of magnetic fields in parallel coupled transmission lines. A number of attenuation poles are produced at 0.8, 1.5, 4.3, 5 and 6.5 GHz, which contribute to sharper selectivity in both bands. Moreover, source–load coupling separates the double attenuation pole at 3 GHz in Fig. 9 and moves them slightly outward such that two attenuation poles appear between the passbands in Fig. 10.

In order to demonstrate the flexibility of the wide dual-band filter design approach, another dual-band filter on a different substrate material (RT6010) and the same height as the former examples is designed at a higher midband frequency ($f_0 = 7$ GHz). The filter structure as well as the performances obtained from measurements and simulations are depicted in Fig. 11. The centre frequencies of the first and second bands were specified as $f_1 = 5.25$ GHz and $f_2 = 8.85$ GHz ($f_2/f_1 \simeq 1.7$) with 22% (1.5 GHz) bandwidth in each band. Note that two attenuation poles at 6.8 and 7 GHz in the measurement replace the double attenuation pole between the passbands in the computations. This is due to the areas between the low-impedance segments of the SIRs (c.f. Fig. 1*b*), which have been manually enlarged due to an error in the prototyping process.

4 Conclusions

The proposed configurations of SIRs with folded high/low-impedance segments and open-ended coupled-line section are excellent candidates for narrowband and wideband dual-band filter applications in wireless communication systems. The wideband design approach is primarily based on UWB filter designs, but folded quarter-wavelength open-ended high-impedance segments generate attenuation poles in the UWB passband to create two highly isolated bands. Enhanced coupling elements provide larger bandwidths, and resonator folding reduces occupied substrate area.

The narrow dual-band filter design is based on the synthesis of the coupling matrix, which is assumed to be valid for both bands. Parallel quarter-wavelength open-ended electric-coupling segments provide not only the required couplings for both bands but also produce the attenuation poles to isolate the two passbands.

In both design approaches, the next (spurious) resonances of the SIRs can be moved as far as possible towards higher frequencies in order to widen the stopband between the upper passband and the next harmonic band. Moreover, source–load coupling can be applied to both dual-band design approaches. Its effect is to distribute a number of attenuation poles in the lower/upper rejection bands and, additionally, move the attenuation poles between the passbands slightly outwards. This is reflected in sharp passband skirts as well as extended upper stopbands. The simplicity and flexibility of the design approach is demonstrated at various examples covering different substrate materials and frequency bands. Ease of fabrication, compact size, low cost and high performance are the main advantages of the proposed dual-band filter design approach. The measured results of six

prototyped dual-band filters show good agreement with simulations and thus verify the design approach.

5 Acknowledgment

This work was supported by the Natural Sciences and Engineering Research Council of Canada and the TELUS Research Grant in Wireless Communications.

6 References

[1] MACCHIARELLA G., TAMIAZZO S.: 'Design techniques for dual-passband filters', *IEEE Trans. Microw. Theory Tech.*, 2005, **53**, pp. 3265–3271

[2] ZHANG Y., ZAKI K.A., RUIZ-CRUZ J.A., ATIA A.E.: 'Analytical synthesis of generalized multi-band microwave filters'. 2007 IEEE MTT-S Int. Microw. Symp. Dig., Honolulu, USA, June 2007, pp. 1273–1276

[3] SAGAWA M., MAKIMOTO M., YAMASHITA S.: 'Geometrical structures and fundamental characteristics of microwave stepped-impedance resonators'', *IEEE Trans. Microw. Theory Tech.*, 1997, **45**, pp. 1078–1085

[4] KUO J.-T., CHENG H.-S.: 'Design of quasi-elliptic function filters with a dual-passband response', *IEEE Microw. Wirel. Comp. Lett.*, 2004, **14**, pp. 472–474

[5] KUO J.-T., YEH T.-H., YEH C.-C.: 'Design of microstrip bandpass filters with a dual-passband response', *IEEE Trans. Microw. Theory Tech.*, 2005, **53**, pp. 1331–1337

[6] SUN S., ZHU L.: 'Coupling dispersion of parallel-coupled microstrip lines for dual-band filters with controllable fractional pass bandwidths'. 2005 IEEE MTT-S Int. Microw. Symp. Dig., Long Beach, USA, June 2005, pp. 2195–2198

[7] TSAI C.-M., LEE H.-M., TSAI C.-C.: 'Planar filter design with fully controllable second passband', *IEEE Trans. Microw. Theory Tech.*, 2005, **53**, pp. 3429–3439

[8] SUN S., ZHU L.: 'Novel design of dual-band microstrip bandpass filters with good in-between isolation'. Proc. 2005 Asia-Pacific Microw. Conf., Suzhou, China, December 2005, Paper T1.8

[9] HUANG T.-H., CHEN H.-J., CHANG C.-S., CHEN L.-S., WANG Y.-H., HOUNG M.-P.: 'A novel compact ring dual-mode filter with adjustable second-passband for dual-band applications', *IEEE Microw. Wirel. Comp. Lett.*, 2006, **16**, pp. 360–362

[10] MOKHTAARI M., RAMBABU K., BORNEMANN J., AMARI S.: 'Advanced stepped-impedance dual-band filters with wide second stopbands'. Proc. 2007 Asia-Pacific Microw. Conf., Bangkok, Thailand, December 2007, pp. 2285–2288

[11] WANG J., GUO Y.-X., WANG B.Z., ONG L.C.: 'Dual-band stepped-impedance band-pass filter'. Proc. 36th European Microw. Conf., Manchester, UK, October 2006, pp. 902–904

[12] ZHANG H., CHEN K.J.: 'A tri-section stepped-impedance resonator for cross-coupled bandpass filters', *IEEE Microw. Wirel. Comp. Lett.*, 2005, **15**, pp. 401–403

[13] LEE C.-H., HSU C.-I.G., JHUANG H.-K.: 'Design of a new tri-band microstrip BPF using combined quarter-wavelength SIRs', *IEEE Microw. Wirel. Comp. Lett.*, 2006, **16**, pp. 494–596

[14] ZHU L., SUN S., MENZEL W.: 'Ultra-wideband (UWB) bandpass filters using multiple-mode resonator', *IEEE Microw. Wireless Comp. Lett.*, 2005, **15**, pp. 796–798

[15] CHIOU Y.-C., KUO J.-T., CHENG E.: 'Broadband quasi-Chebyshev bandpass filters with multimode stepped-impedance resonators (SIRs)', *IEEE Trans. Microw. Theory Tech.*, 2006, **54**, pp. 3352–3358

[16] MOKHTAARI M., BORNEMANN J., AMARI S.: 'Folded compact ultra-wideband stepped-impedance resonator filters'. 2007 IEEE MTT-S Int. Microw. Symp. Dig., Honolulu, USA, June 2007, pp. 747–750

[17] CAI P., MA Z., GUAN X., KOBAYASHI Y., ANADA T., HAGIWARA G.: 'A novel compact ultra-wideband bandpass filter using a microstrip stepped-impedance four-modes resonator'. 2007 IEEE MTT-S Int. Microw. Symp. Dig., Honolulu, USA, June 2007, pp. 751–754

[18] LEE S.-Y.: 'Optimum resonant conditions of stepped impedance resonators'. Proc. 35th European Microw. Conf., Paris, France, October 2005, pp. 417–420

[19] MOKHTAARI M., BORNEMANN J., AMARI S.: 'Dual-band stepped-impedance filters for ultra-wideband applications'. Proc. 37th European Microw. Conf., Munich, Germany, October 2007, pp. 779–782

[20] MOKHTAARI M., BORNEMANN J., AMARI S.: 'Quasi-elliptic dual-band stepped-impedance filters with folded parallel high-impedance segments'. Proc. 37th European Microw. Conf., Munich, Germany, October 2007, pp. 862–865

[21] WADELL B.C.: 'Transmission line design handbook', (Artech House, Boston, 1991)

doi: 10.1049/iet-map:20070352